Journal of Power Sources 192 (2009) 63–69

Contents lists available at ScienceDirect

Journal of Power Sources

journal homepage: www.elsevier.com/locate/jpowsour

Synthesis and electrochemical performance of $La_{0.6}Ca_{0.4}Fe_{1-x}Ni_xO_3$ ($x = 0.1, 0.2, 0.3$) material for solid oxide fuel cell cathode

N. Ortiz-Vitoriano, I. Ruiz de Larramendi, J.I. Ruiz de Larramendi, M.I. Arriortua, T. Rojo *

Departamento de Química Inorgánica, Facultad de Ciencia y Tecnología, Universidad del País Vasco, Apdo. 644, 48080 Bilbao, Spain

ARTICLE INFO

Article history:
Received 15 October 2008
Received in revised form
27 November 2008
Accepted 1 December 2008
Available online 7 December 2008

Keywords:
Solid oxide fuel cell
Cathode
Perovskite
Electrochemical impedance spectroscopy

ABSTRACT

Polycrystalline samples of $La_{0.6}Ca_{0.4}Fe_{1-x}Ni_xO_3$ ($x = 0.1, 0.2, 0.3$) (LCFN) are prepared by liquid mix method. The structure of the polycrystalline powders is analyzed with X-ray powder diffraction data. The XRD patterns are indexed as the orthoferrite similar to that of $LaFeO_3$ having a single phase with orthorhombic perovskite structure (*Pnma*). The morphological characterization is performed by scanning electron microscopy (SEM) obtaining a mean particle size less than 300 nm.

Polarization resistance is studied using two different electrolytes: Y-stabilized zirconia (YSZ) and Sm-doped ceria (SDC). Electrochemical impedance spectroscopy (EIS) measurements of LCFN/YSZ/LCFN and LCFN/SDC/LCFN test cells are carried out. These electrochemical experiments are performed at equilibrium from 850 °C to room temperature, under both zero dc current intensity and air. The best value of area specific resistance (ASR) obtained is 0.88 Ω cm^2, corresponding to the $La_{0.6}Ca_{0.4}Fe_{0.9}Ni_{0.1}O_3$ material using SDC as electrolyte. The dc four-probe measurement indicates that $La_{0.6}Ca_{0.4}Fe_{0.9}Ni_{0.1}O_3$ exhibits fairly high electrical conductivity, over 300 S cm^{-1} at $T > 500$ °C.

1. Introduction

Solid oxide fuel cells (SOFCs) are considered promise devices to convert energy that exhibit main advantages such as high efficiency and low environmental impact [1]. The energy conversion is direct without any intermediate phase. The most common materials for the SOFC are oxide ion conducting yttria-stabilized zirconia (YSZ) for the electrolyte, strontium-doped lanthanum magnanite (LSM) for the cathode, nickel/YSZ cerment for the anode, and doped lanthanum chromite or refractory metals as interconnect materials [2].

Sr-doped $LaMnO_3$ (LSM) has been widely studied for decades as a cathode material, primarily due to its relatively high electrocatalytic activity for O_2 reduction and good thermal and chemical compatibility with Y_2O_3-stabilized ZrO_2 electrolyte [3]. Chemical reactivity at high temperatures between LSM and YSZ leads to the formation of the pyrochlore, $La_2Zr_2O_7$ (LZO). The formation of LZO reduces cathode performance because it has significantly lower conductivity than LSM or YSZ at fuel cell operating temperatures [4].

The traditional SOFC operated at high temperature up to 1000 °C presents some problems related to the cost of the materials and fabrication. Therefore, an important research is to get lower cost components for operation temperatures under 800 °C [5]. So, new materials exhibiting good performance at lower temperatures for conductivity, chemical and mechanical compatibility should be obtained.

Perovskite oxides have general formula ABO_3 where A site may be occupied by rare earth, alkaline-earth, alkali or other large ions and B sites are usually filled with transition metal cations [6]. They have attracted much attention because of their utility in several electrochemical processes such as SOFCs, oxygen sensors and membranes for oxygen separation. Cathode of SOFCs should have high-electronic and ionic conductivities, adequate porosity, thermal and chemical compatibilities with the electrolyte, and long-term stability [7]. In this way, mixed ionic and electronic conductors (MIECs) exhibit main advantages [8].

In the $Ln_{1-x}A_xFeO_3$ (Ln = lanthanides and A = alkaline-earth) system when Fe is substituted by other transition metal ions, interesting transport properties have been observed. In this way, when the Fe fraction is higher than 0.5 the materials exhibit a high electronic conductivity as was observed for the $La_{0.6}Sr_{0.4}Fe_{0.8}Ni_{0.2}O_3$ phase in which a conductivity of 435 S cm^{-1} at 800 °C was obtained [9,10]. Otherwise, it is known that $LaNiO_3$ has a very high electronic conductivity at room temperature. Calcium is another effective doping-element at the A-site of ABO_3, with lower cost [11]. Moreover, calcium could be a good candidate because of the similarity of its ionic radius with La^{3+} which could give rise to higher stability than that of strontium substituted phases [6].

* Corresponding author. Tel.: +34 94 6012458; fax: +34 94 6013500.
E-mail address: teo.rojo@ehu.es (T. Rojo).

0378-7753/$ – see front matter.
doi:10.1016/j.jpowsour.2008.12.009

This paper reports the influence on the electrochemical properties of the Ni content in the B-site of the $La_{0.6}Ca_{0.4}Fe_{1-x}Ni_xO_3$ perovskite and the effect of iron substitution by nickel on the electronic and ionic conduction. This material was synthesized, and characterized by powder X-ray diffraction and scanning electron microscopy (SEM). The electrochemical impedance spectroscopy (EIS) measurements performed in symmetrical cells with two different electrolytes (Y-stabilized zirconia and Sm-doped ceria, SDC) and dc four-probe measurements on sintered bars are described.

2. Experimental

Powders of $La_{0.6}Ca_{0.4}Fe_{1-x}Ni_xO_3$ ($x = 0.1$, 0.2, 0.3) (LCFN in the following) with perovskite structure were prepared by the liquid mix process. Appropriate amounts of the nitrate salts [$La(NO_3)_3{\cdot}6H_2O$; $Ca(NO_3)_2{\cdot}H_2O$; $Fe(NO_3)_3{\cdot}9H_2O$; $Ni(NO_3)_2{\cdot}6H_2O$] and citric acid were dissolved in distilled water and later a suitable volume of ethylene glycol was added. The resulting solution was agitated and heated in a heating plate until the formation of a gel. After that the gel, which was already treated in a sand bath, was calcined at 600 °C in an oven for 12 h with a 1° min^{-1} rate.

The powders were characterized by X ray powder diffraction data, collected using a Philips PW1710 and Philips X'Pert-MPD (Bragg-Brentano geometry) diffractometers, with Cu Kα radiation, and fitted using the FULLPROF program [12]. The microstructure of the samples was observed by SEM using a JEOL JSM-6400 microscope at 20 kV accelerating voltage. The chemical compatibility of the proposed materials as cathode electrode was studied with two different electrolytes: YSZ and SDC.

EIS measurements of LCFN/YSZ/LCFN and LCFN/SDC/LCFN test cells were conducted using a Solartron 1260 Impedance Analyzer. The frequency range was 10^{-2} to 10^6 Hz with a signal amplitude of 50 mV. All these electrochemical experiments were performed at equilibrium from 850 °C to room temperature, under zero dc current intensity and under air over a cycle of heating and cooling. Impedance diagrams were analysed and fitted using the Zview software. Resistance, capacitance and self-values of equivalent circuits were thus obtained by least square refinement.

The electrical conductivity of sintered bars was measured in air from 500 to 800 °C at 100 °C intervals by a dc four-probe technique. Electrical contacts were made using Pt wires and Pt paste placed over whole end faces ensuring a homogeneous current flow.

3. Results and discussion

The powder XRD patterns for the $La_{0.6}Ca_{0.4}Fe_{1-x}Ni_xO_3$ ($x = 0.1$, 0.2, 0.3) samples are plotted in Fig. 1, and the lattice parameters are summarized in Table 1. The analysis of these data revealed that the samples are single phases, presenting orthorhombic perovskite structure (space group *Pnma*), similar to those of $LaFeO_3$ [13] and $Ln_{0.6}Ca_{0.4}FeO_3$ [11]. The effect of doping with calcium and nickel induces a distortion of the structure, but structural transitions are not observed in these phases which are usually found in this type of systems [14].

The tolerance factors (τ) for these samples (calculated using Shannon ionic radii [15]) are also shown in Table 1. Although for an ideal perovskite the value of the tolerance factor is unity, with lower τ values the perovskite structure is found to be distorted to tetragonal, rhombohedral, orthorhombic or monoclinic symmetry [16,17]. On having doped with calcium the lanthanum site and with nickel the iron one, an improvement of the value of the tolerance factor respect to that of $LaFeO_3$ phase ($\tau = 0.9605$) is obtained. It is well known that the perovskite structure becomes more stable when the amount of Fe is higher than Ni [9]. This means that the substitution of Fe by Ni increases the thermodynamic stability of this material and the thermal expansion coefficient is close to that

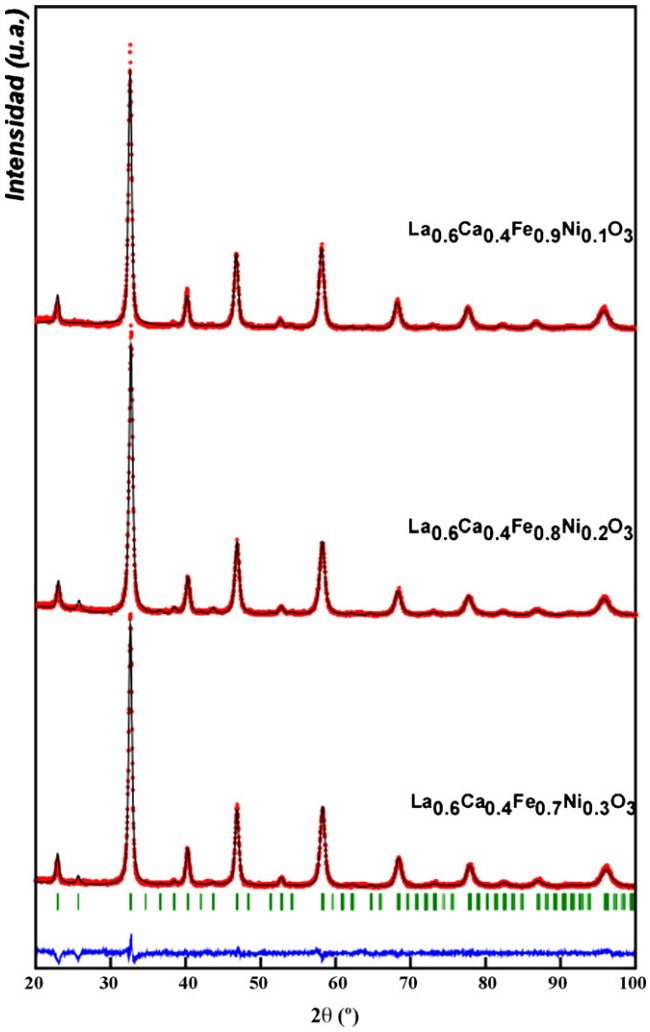

Fig. 1. XRD patterns of $La_{0.6}Ca_{0.4}Fe_{1-x}Ni_xO_3$ powders: (a) $x = 0.1$, (b) $x = 0.2$ and (c) $x = 0.3$ (experimental, squares; fitted, line; and difference between them, lower line).

of the zirconia and ceria electrolytes [18]. Furthermore, Hrovat et al. [19] showed that $LaNiO_3$ was stable at high temperatures when some of the Ni ions are substituted. In this work, the perovskite structure is more stable for the 30% nickel phase.

In order to get the particle size of the samples, SEM measurements were carried out. It is well known that the particle size influences on conductive properties of the sample. Therefore, particle size must be reduced in order to obtain a better behaviour of the material as cathode. The SEM micrographs of the LCFN samples are shown in Fig. 2. The grain size is heterogeneous, from agglomerates (10 μm) to free particles less than 300 nm. The particle size in the samples is practically similar but smaller for the 20% nickel phase.

A requirement for the successful operation of SOFC is the mechanical stability of the cathode with respect to the electrolyte [7]. In this way, the chemical reactivity between the

Table 1
Unit cell parameters, volume and tolerance factors (τ) of the $La_{0.6}Ca_{0.4}Fe_{1-x}Ni_xO_3$ samples.

	$x = 0.1$	$x = 0.2$	$x = 0.3$
a (Å)	5.509 (2)	5.513 (2)	5.491 (2)
b (Å)	7.778 (2)	7.779 (2)	7.752 (2)
c (Å)	5.501 (2)	5.505 (2)	5.482 (1)
V (Å^3)	235.8 (1)	236.1 (1)	233.3 (1)
τ	0.9714	0.9738	0.9760

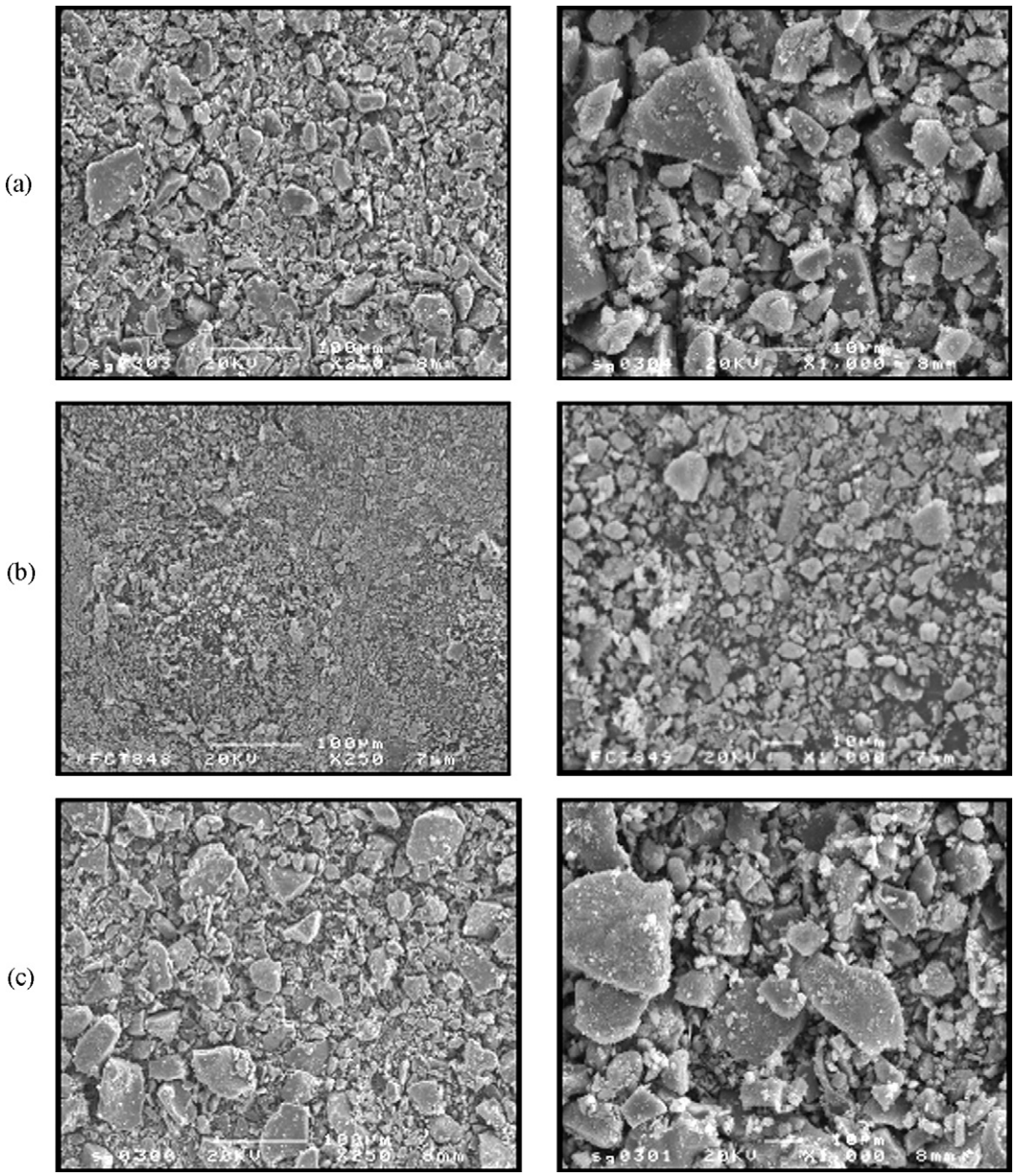

Fig. 2. SEM micrographs of $La_{0.6}Ca_{0.4}Fe_{1-x}Ni_xO_3$ samples: (a) $x = 0.1$, (b) $x = 0.2$ and (c) $x = 0.3$.

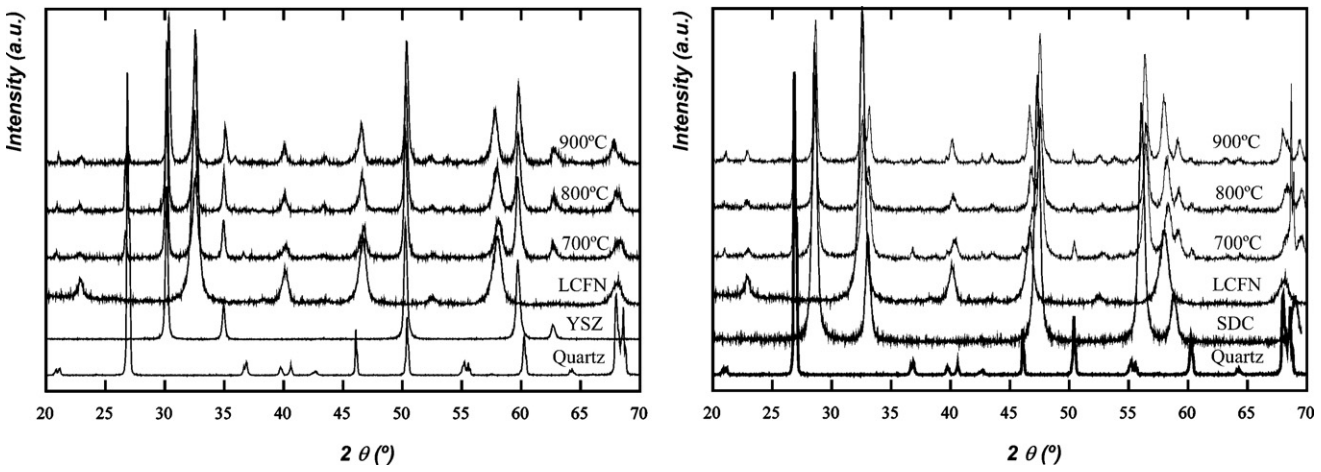

Fig. 3. X-ray diffraction patterns of equimolecular $La_{0.6}Ca_{0.4}Fe_{0.8}Ni_{0.2}O_3$/electrolyte material mixtures after annealing in air at different temperatures for 1 week: (a) YSZ and (b) SDC.

$La_{0.6}Ca_{0.4}Fe_{1-x}Ni_xO_3$ (x = 0.1, 0.2, 0.3) materials and two electrolytes, YSZ and SDC, has been studied. Cathode materials and electrolyte powders were intimately mixed together (1/1 mass ratio) and isopressed to form a pellet. These pellets were sintered at different temperatures for 1 week. Quartz was used as standard material. XRD patterns of the chemical reactivity test are shown in Fig. 3. No main reaction products were formed between the perovskite oxide materials and SDC electrolyte after all annealing temperatures. On the other hand, for the YSZ electrolyte at 900 °C some small peaks were found but it was not possible to assign them to any reaction product.

The study of the conducting properties was carried out using a two-electrode cell, being necessary to obtain the impedance spectra for symmetrical cells. In this way, the cells were made of electrolyte pellets onto which were deposited symmetrical electrodes. Two different commercial electrolytes (SDC and YSZ) have been used. Platinum was utilized as current collector.

The SDC and YSZ pellets were made using Nextech materials as they were received. The powder of each material was pressed under 10-T uniaxial force to form green pellets. The pellets were sintered at 1500 °C for 2 h. The density of the obtained pellets is higher than 93% opposite to the theoretical value. The surface of the pellets was polished with grit paper and then cleaned with ethanol and acetone solutions.

In order to prepare the electrodes, the obtained powders were grinded. After that, the powder was dispersed in a vehicle ink in a 1:1 weight proportion forming a paste. This paste was painted with a paintbrush in both faces of the pellets forming symmetrical cells. These cells were sintered at 1050 °C for 1 h with a 10 °C min^{-1} rate to form porous electrodes well adhered to the surface of the electrolytes.

Nyquist plot of LCFN/YSZ/LCFN cell measured at 300 °C, in air, is shown in Fig. 4. In this figure, the different processes observed at low temperatures are described. The semicircle at high frequencies corresponding to the bulk of the compound shows a value of capacitance of 1.37×10^{-12} F which is in good agreement with those described in the literature [20]. The following semicircle that is observed at middle frequencies is due to the grain boundary contribution of the electrolyte, with a value of capacitance of 2.03×10^{-7} F. This value can be assigned to the contribution of the interface between sample and electrode, which is important due to the impedance response can give information on the nature of the conducting species (ions or electrons). Later, at medium and lower frequencies the semicircles due to the different processes taking place in the electrode (interface processes, electrode reactions, etc.) appear; however, this contribution is better observed at high temperatures.

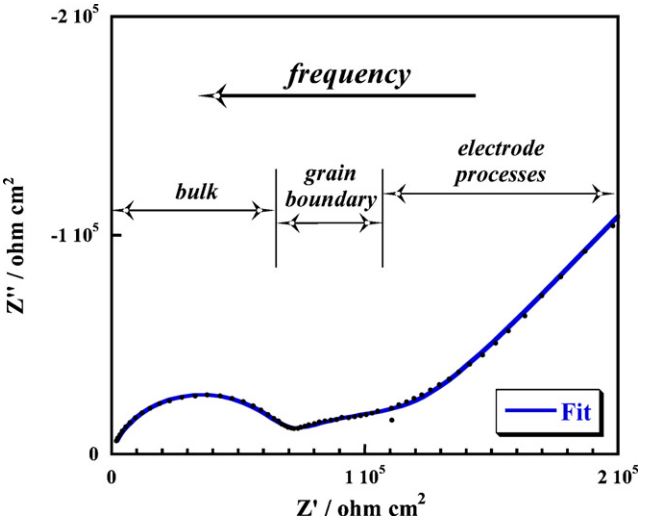

Fig. 4. Typical impedance diagram obtained with LCFN/YSZ half-cells, under air, at 300 °C for the sample $La_{0.6}Ca_{0.4}Fe_{0.7}Ni_{0.3}O_3$.

Typical electrochemical impedance spectra for LCFN/YSZ/LCFN ($La_{0.6}Ca_{0.4}Fe_{0.8}Ni_{0.2}O_3$ sample) and LCFN/SDC/LCFN ($La_{0.6}Ca_{0.4}Fe_{0.7}Ni_{0.3}O_3$ sample) cells are reported in the Nyquist plan at 800 °C (Fig. 5). The equivalent circuit used to fit the measured impedance spectra at low frequency is also shown. The Nyquist plots were fitted on the basis of an equivalent circuit constituted of resistance-constant phase elements (R-CPE) in parallel associated in series. Each resistance or CPE can be assigned to the resistance or capacitance associated with a specific electrochemical process. The R_{elyte} element was assigned to the electrochemical resistance due to the different electrolytes. In case of the sample with SDC the resistance is lower than that of YSZ. Likewise, using SDC as electrolyte, two electrodic processes are distinguished. The high frequency arc could be attributed to the oxygen ion transference from the electrode-electrolyte interface into the electrolyte and the low frequency arc could be assigned to the charge transfer process and oxygen diffusion process. This process is overlapped with YSZ being more complicated to distinguish the contribution of each one.

The Arrhenius plots of capacitances and relaxation frequencies of the different contributions are shown in Figs. 6 and 7. A study according to the methodology proposed by Schouler et al. [21] was carried out. The thermal evolution of the relaxation frequencies, f_r, is independent of the geometric characteristics of the sample, being able to associate the different contributions to their respective processes.

Using this study, the different electrolyte contributions, which are only detected at low temperatures, were observed at high frequencies. The contributions at higher frequencies correspond to that of the bulk, whereas those indicated as *gb* are associated to the processes carried out in the grain boundary. The capacitance values assigned to the electrolyte bulk and grain boundary processes are 10^{-12} F cm^{-3} and 10^{-9} F cm^{-3}, respectively. These capacitance values and the associated relaxation frequencies are in good agreement with those given in the literature for analogous phases [21]. On the other hand, at low frequencies a big difference between both electrolytes is appreciated. In the case of YSZ, only the cathode process is observed. This fact can be attributed to the several overlapped processes which were not possible to distinguish clearly and agree with those reported in the literature [22]. We perform in the study on the SDC a new contribution to intermediate frequencies that is associated with the behaviour of MIEC [23]. The oxygen reduction mechanism on porous MIEC electrodes may involve several processes such as charge transfer at the current collector/electrode interface and electrode/electrolyte interfaces, oxygen exchange at the electrode surface, bulk and surface diffusion of oxygen species and gas phase diffusion. To be able to assign every contribution with its respective semicircle, measurements in different oxygen partial pressures should be performed. So, a clear identification of these contributions was not possible in this work.

The cathodic area specific resistance (ASR) was deduced from the relation: ASR = $R_{electrode}$·surface/2. The Arrhenius plots of the ASR values for LCFN/SDC/LCFN and LCFN/YSZ/LCFN half-cells, using the $La_{0.6}Ca_{0.4}Fe_{0.9}Ni_{0.1}O_3$ sample, are given in Fig. 8. The electrochemical measurements showed a better performance for the SDC electrolyte (with an ASR value at 850 °C of 0.88 Ω cm^2) than that of the YSZ (65.15 Ω cm^2 at 850 °C).

The Arrhenius plots of the ASR values for $La_{0.6}Ca_{0.4}Fe_{1-x}Ni_xO_3$ (x = 0.1, 0.2, 0.3) with SDC electrolyte are shown in Fig. 9. When x = 0.2 and 0.3, ASR values remain over 1 Ω cm^2. On the other hand, the $La_{0.6}Ca_{0.4}Fe_{0.9}Ni_{0.1}O_3$ sample presents the minor ASR being this of 0.88 Ω cm^2 at 850 °C. The values obtained for the

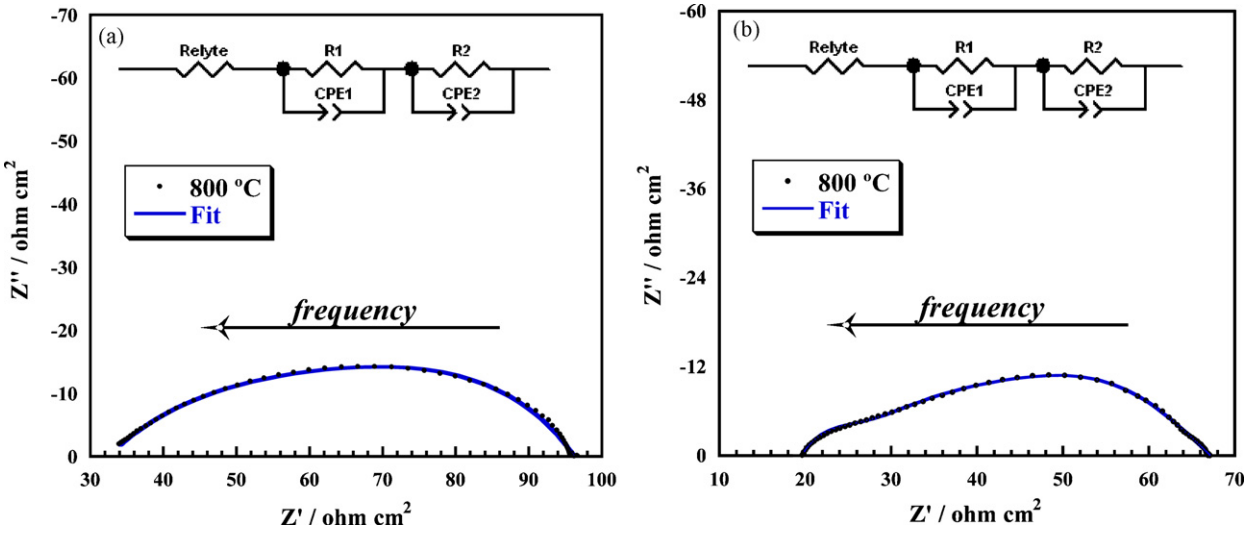

Fig. 5. Typical impedance spectra measured at 800 °C (inset: equivalent circuit used for fitting data), under air: (a) YSZ ($La_{0.6}Ca_{0.4}Fe_{0.8}Ni_{0.2}O_3$ sample) and (b) SDC ($La_{0.6}Ca_{0.4}Fe_{0.7}Ni_{0.3}O_3$ sample). The impedance data are plotted after electrolyte ohmic drop correction.

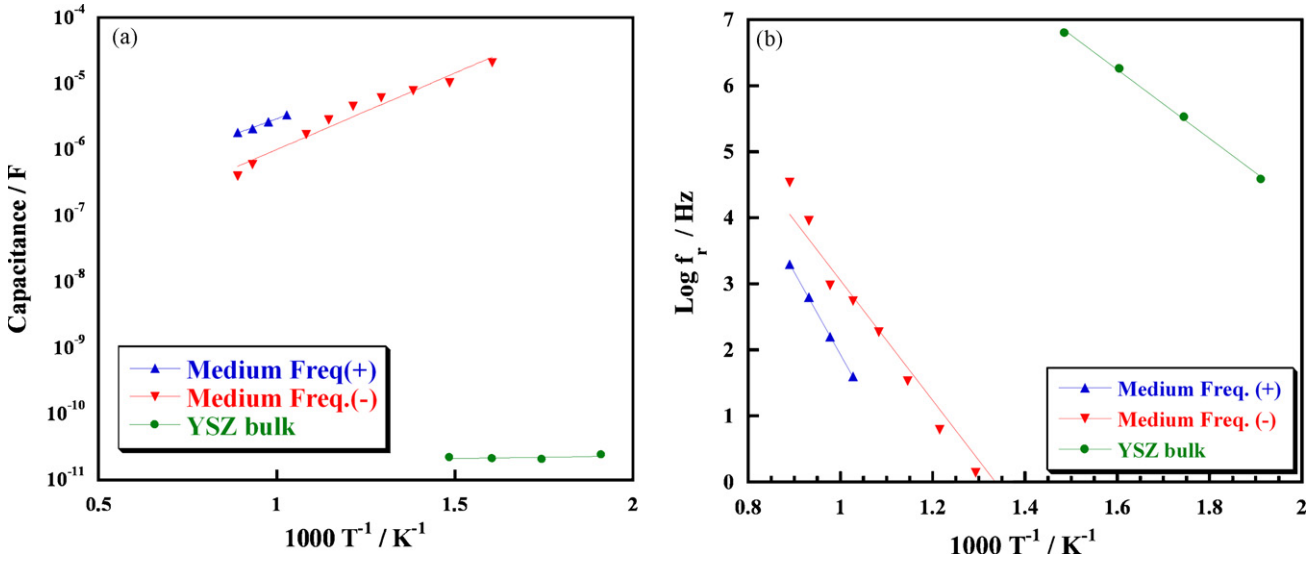

Fig. 6. Arrhenius plots of (a) capacitances and (b) relaxation frequencies for the LCFN/YSZ/LCFN cells under air and zero dc conditions for $La_{0.6}Ca_{0.4}Fe_{0.7}Ni_{0.3}O_3$ sample.

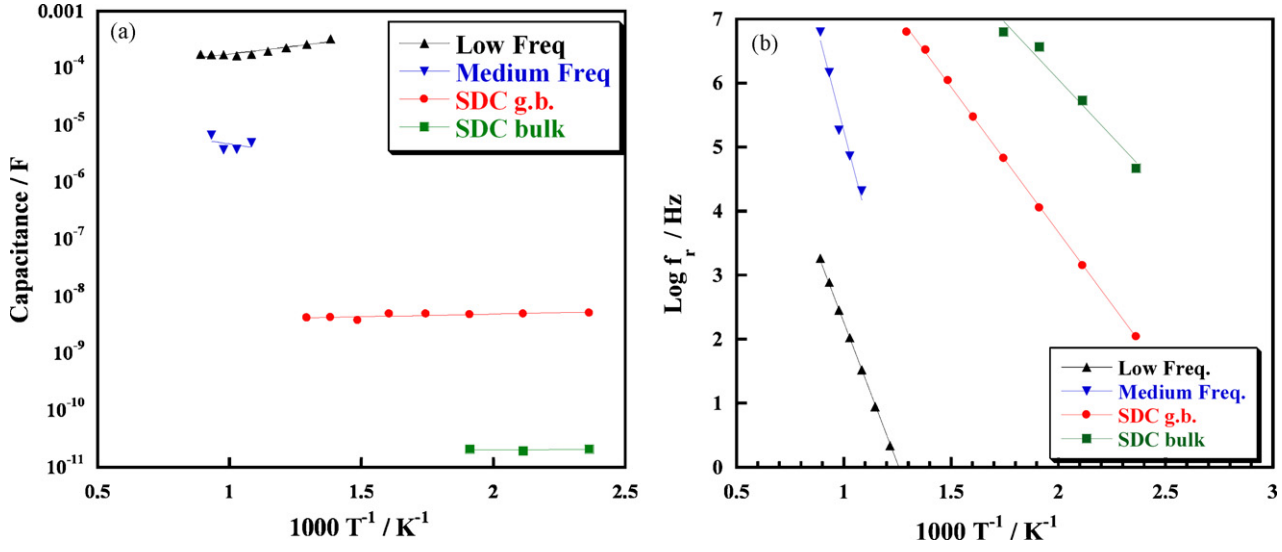

Fig. 7. Arrhenius plots of (a) capacitances and (b) relaxation frequencies for the LCFN/SDC/LCFN cells under air and zero dc conditions for $La_{0.6}Ca_{0.4}Fe_{0.9}Ni_{0.1}O_3$ sample.

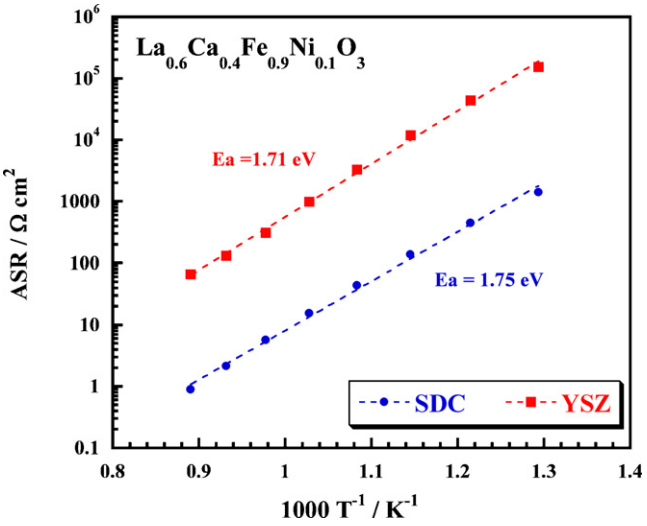

Fig. 8. Arrhenius plots of ASR for $La_{0.6}Ca_{0.4}Fe_{0.9}Ni_{0.1}O_3$ electrode with two different electrolytes.

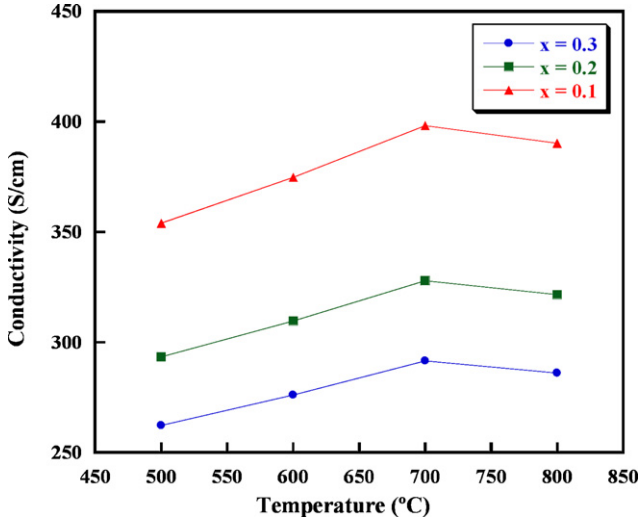

Fig. 10. Conductivity dependence upon the temperature for $La_{0.6}Ca_{0.4}Fe_{1-x}Ni_xO_3$ ($x = 0.1, 0.2, 0.3$) samples.

$La_{0.6}Ca_{0.4}Fe_{0.8}Ni_{0.2}O_3$ and $La_{0.6}Ca_{0.4}Fe_{0.7}Ni_{0.3}O_3$ phases at 850 °C are 5.73 and 10.12 Ω cm^2, respectively. As the Ni content is decreased, the resistance associated to the material is lower. The resistance of all the materials increased linearly with decreasing temperature, showing similar activation energy for the conduction process as was observed for the $La_{0.6}Ca_{0.4}Mn_{1-y}Ni_yO_3$ system [24]. These results agree with a hopping of small polarons as dominating mechanism for the electrical conduction.

Alternatively, the $SrCo_{0.8}Fe_{0.2}O_3$ (SCF) mixed conductor has been reported in the literature as a competitive cathode [25], having the highest ionic conductivity of the $La_{1-x}Sr_xCo_{1-y}Fe_yO_3$ system [26]. Using SCF with $La_{0.45}Ce_{0.55}O_{2-\delta}$ (LDC) as electrolyte the obtained ASR values are slightly lower than those presented in this paper [27]. However, cobalt is an expensive element and perovskite cathodes containing Sr might be unstable on repeated thermal cycling [28]. Taking into account these considerations, although $La_{0.6}Ca_{0.4}Fe_{0.9}Ni_{0.1}O_3$ presents a resistance slightly higher, its great stability and low chemical interaction turn it into an interesting option as cathode for intermediate temperature SOFC.

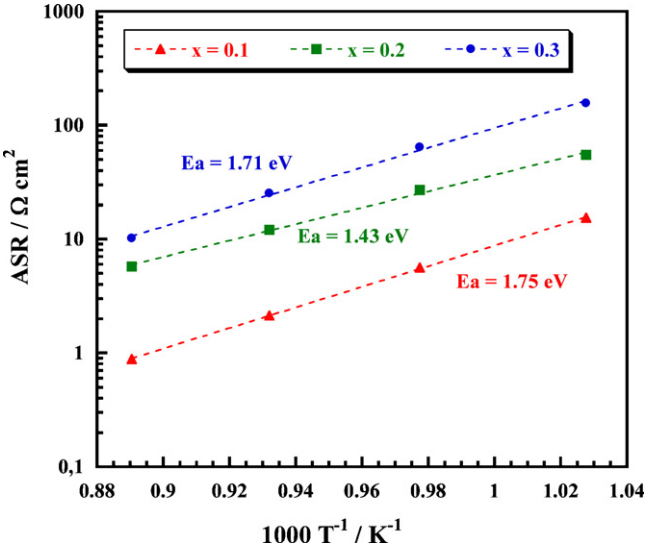

Fig. 9. Arrhenius plots of ASR for $La_{0.6}Ca_{0.4}Fe_{1-x}Ni_xO_3$ ($x = 0.1, 0.2, 0.3$) electrodes with SDC electrolyte.

The total electrical conductivity as a function of temperature measured by the four-point method is shown in Fig. 10. As it can be seen in this figure, the best obtained value corresponds to the $La_{0.6}Ca_{0.4}Fe_{0.9}Ni_{0.1}O_3$ phase. It is worth mentioning that the electrical conductivities of the $La_{0.6}Ca_{0.4}Fe_{1-x}Ni_xO_3$ ($x = 0.1$, 0.2, 0.3) samples are 390.15, 321.57 and 286.16 S cm^{-1} at 800 °C, respectively. These values are well over 100 S cm^{-1} including when $T \geq 500$ °C, the general requirement for electrode materials in intermediate temperature SOFC. This result is comparable to that of $La_{1-x}Sr_xFe_{1-y}Ni_yO_3$ ($x = 0.3$, $y = 0.1$) which exhibits the highest conductivity [29]. Normally, the Fe and Ni-based perovskites [30,31] exhibit structural defects as oxygen vacancies and elevated electronic conductivity, showing mixed oxygen ionic and electrical conductivities. This is due to the formation of anionic vacancies. These vacancies appear easier than the oxidation of Ni^{3+} to Ni^{4+}, since the ionic radius of oxidised species does not fit to the perovskite structure. This is the reason for what the electrical conductivity diminishes as the Ni content increases.

4. Conclusions

The $La_{0.6}Ca_{0.4}Fe_{1-x}Ni_xO_3$ ($x = 0.1$, 0.2, 0.3) phases were characterized by powder X-ray diffraction with an orthorhombic perovskite-type structure. The particle size was studied by scanning electron microscopy obtaining an inhomogeneous particle size and agglomerates. The electrochemical measurements showed a better performance for both the SDC electrolyte and the sample with 10% of nickel exhibiting an ASR value of 0.88 Ω cm^2 at 800 °C which was measured in a two-electrode configuration using symmetrical cells. The electrical conductivities of the $La_{0.6}Ca_{0.4}Fe_{1-x}Ni_xO_3$ ($x = 0.1$, 0.2, 0.3) phases at $T \geq 500$ °C are well over 100 S cm^{-1}, indicating that these materials are of interest to be considered as electrodes in intermediate temperature SOFC devices.

Acknowledgements

This work has been partially financed by the Spanish CiCyT under project MAT2007-66737-C02-01 and by the Government of the Basque Country under project IT-312-07. N. Ortiz-Vitoriano thanks the Eusko Jaurlaritza/Gobierno Vasco for a predoctoral fellowship.

References

[1] J. Liu, A.C. Co, S. Paulson, V.I. Birss, Solid State Ionics 177 (2006) 377–387.
[2] I. Ruiz de Larramendi, R.L. Antón, J.I. Ruiz de Larramendi, S. Baliteau, F. Mauvy, J.C. Grenier, T. Rojo, J. Power Sources 169 (2007) 35–39.
[3] W. Wang, S.P. Jiang, Solid State Ionics 177 (2006) 1361–1369.
[4] C. Chervin, R.S. Glass, S.M. Kauzlarich, Solid State Ionics 176 (2005) 17–23.
[5] M.H. Hung, M.V. Madhara, D.S. Tsai, Mater. Chem. Phys. 101 (2007) 297–302.
[6] P. Ciambelli, S. Cimino, L. Lisi, M. Faticanti, G. Minelli, I. Pettiti, P. Porta, Appl. Catal. B: Environ. 33 (2001) 193–203.
[7] G. Zhu, X. Fang, C. Xia, X. Liu, Ceram. Int. 31 (2005) 115–119.
[8] M.A. Ahmed, S.I. El-Dek, Mater. Sci. Eng. B 128 (2006) 30–33.
[9] R. Chiba, F. Yoshimura, Y. Sakurai, Solid State Ionics 152–153 (2002) 575–582.
[10] R. Chiba, F. Yoshimura, Y. Sakurai, Solid State Ionics 124 (1999) 281–288.
[11] Y.H. Chen, Y.J. Wei, H.H. Zhong, J.F. Gao, X.Q. Liu, G.Y. Meng, Ceram. Int. 33 (2007) 1237–1241.
[12] J. Rodriguez-Carvajal, Physica B 192 (1993) 55–69.
[13] A. Jones, M.S. Islam, J. Phys. Chem. C 112 (2008) 4455–4462.
[14] K. Vidal, L.M. Rodríguez-Martínez, L. Ortega-San-Martin, E. Díez-Linaza, M.L. Nó, T. Rojo, A. Laresgoiti, M.I. Arriortua, Solid State Ionics 178 (2007) 1310–1316.
[15] R.D. Shannon, Acta Crystalogr. A 32 (1976) 751–767.
[16] M.A. Peña, J.L.G. Fierro, Chem. Rev. 101 (2001) 1981–2017.
[17] C.N.R. Rao, J. Gopalakrishnan, New Directions in Solid State Chemistry, Cambridge University Press, Cambridge, 1989.
[18] X. Chen, N.J. Wu, A. Ignatiev, J. Eur. Ceram. Soc. 19 (1999) 819–822.
[19] M. Hrovat, N. Katsarakis, K. Reichmann, S. Bernik, D. Kuscer, J. Holc, Solid State Ionics 83 (1996) 99–105.
[20] X. Chen, N.J. Wu, D.L. Ritums, A. Ignatiev, Thin Solid Films 342 (1999) 61–66.
[21] E.J.L. Schouler, N. Mesbahi, G. Vitter, Solid State Ionics 9 & 10 (1983) 989–996.
[22] J.T.S. Irvine, D.C. Sinclair, R. West, Adv. Mater. 2 (3) (1990) 132–138.
[23] C. Lalanne, PhD thesis, UB1 Bordeaux, 2005.
[24] V. Vashook, D. Franke, L. Vasylechko, J. Zosel, J. Rebello, K. Ahlborn, W. Fichtner, M. Schmidt, T.-L. Wen, U. Guth, Solid State Ionics 179 (21) (2008) 1101–1107.
[25] K. Huang, J. Wan, J.B. Goodenough, J. Mater. Sci. 6 (2001) 1093–1098.
[26] Y. Teraoka, H. Zhang, K. Okamoto, Mater. Res. Bull. 23 (1) (1998) 51–58.
[27] X.D. Zhu, K.N. Sun, N.Q. Zhang, X.B. Chen, L.J. Wu, D.C. Jia, Electrochem. Commun. 9 (2007) 431–435.
[28] J. Wan, J.B. Goodenough, J.H. Zhu, Solid State Ionics 178 (2007) 281–286.
[29] Y. Wu, T. Yu, B.S. Dou, C.X. Wang, X.F. Xie, Z.L. Yu, S.R. Fan, Z.R. Fan, L.C. Wang, J. Catal. 120 (1989) 88–107.
[30] V.V. Kharton, A.A. Viskupa, E.N. Naumovicha, V.N. Tikhonovicha, Mater. Res. Bull. 34 (1999) 1311–1317.
[31] K. Huang, H.Y. Lee, J.B. Goodenough, J. Electrochem. Soc. 145 (8) (1998) 3220–3227.